THE JOURNAL OF PHYSICAL CHEMISTRY Letters

Letter

pubs.acs.org/JPCL

Shrinking the Synchrotron: Tabletop Extreme Ultraviolet Absorption of Transition-Metal Complexes

Kaili Zhang,[†] Ming-Fu Lin,[†] Elizabeth S. Ryland,[†] Max A. Verkamp,[†] Kristin Benke,[†] Frank M. F. de Groot,[‡] Gregory S. Girolami,[†] and Josh Vura-Weis*[,†]

[†]Department of Chemistry, University of Illinois at Urbana-Champaign, Champaign 61801, United States

[‡]Department of Chemistry, Utrecht University, 3584 CG Utrecht, The Netherlands

Supporting Information

ABSTRACT: We show that the electronic structure of molecular first-row transition-metal complexes can be reliably measured using tabletop high-harmonic XANES at the metal $M_{2,3}$ edge. Extreme ultraviolet photons in the 50−70 eV energy range probe 3p → 3d transitions, with the same selection rules as soft X-ray $L_{2,3}$-edge absorption (2p → 3d excitation). Absorption spectra of model complexes are sensitive to the electronic structure of the metal center, and ligand field multiplet simulations match the shapes and peak-to-peak spacings of the experimental spectra. This work establishes high-harmonic spectroscopy as a powerful tool for studying the electronic structure of molecular inorganic, bioinorganic, and organometallic compounds.

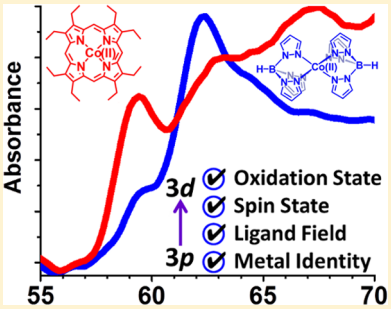

X-ray absorption near edge spectroscopy (XANES or NEXAFS) is a powerful technique for measuring the electronic structure of transition-metal complexes and has played a pivotal role in elucidating the structure and function of metalloproteins,[1] coordination complexes,[2] semiconductors,[3] and catalysts.[4] First-row transition metals are most commonly studied at the K edge (5−10 keV), corresponding to 1s → valence transitions. Dipole selection rules allow excitation into molecular orbitals with contributions from the metal 4p orbitals, while a quadrupole transition allows direct 1s → 3d excitation and is sensitive to the symmetry and covalency of the metal center. Oscillations of the absorption above the edge provide a high-resolution structural probe of the local environment via extended absorption fine structure (EXAFS) spectroscopy. $L_{2,3}$-edge absorption measures dipole-allowed 2p → 3d transitions in the 500−1000 eV region. This edge provides stronger absorption than the K edge, greater sensitivity to spin states, and narrower line widths due to a longer core-hole lifetime. These advantages are balanced by a shorter penetration depth (∼1 μm) and the need for a high-vacuum sample environment to avoid absorption by air. Time-resolved versions of each of these techniques have been used to determine the structure of short-lived intermediates in catalytic and photochemical systems.[5−9]

K-edge and $L_{2,3}$-edge spectroscopy are generally performed using synchrotron radiation or free-electron laser facilities, with the latter providing femtosecond time resolution and extremely high flux. Over the past 10 years, the development of tabletop extreme ultraviolet (XUV) and X-ray light sources has enabled core-level spectroscopy to be performed on femtosecond to attosecond time scales.[10−16] High-energy OPCPA instruments can reach keV energies using high-harmonic generation (HHG) or metal plasma techniques.[17,18] HHG using few-millijoule Ti:sapphire lasers can routinely produce XUV photons in the 50−100 eV spectral range corresponding to the $M_{2,3}$ edge, or 3p → 3d transition, of first-row transition metals. Given the ubiquity of such lasers in ultrafast laboratories and the availability of femtosecond XUV free-electron lasers such as FLASH,[19] we sought to explore whether spectroscopy in this underexplored region could complement more established techniques at the K and L edges. The oscillator strength at the M edge is ∼10 times higher than at the L edge and 1000 times higher than at the K edge. This is potentially advantageous for pump/probe spectroscopy because the penetration depth for the visible pump and XUV/X-ray probe are better matched.[14]

In this work, we demonstrate that $M_{2,3}$-edge XANES can reliably measure the electronic structure of first-row transition-metal coordination complexes. Furthermore, simulations of the spectra, using a semiempirical ligand field multiplet method developed for the $L_{2,3}$ edge, provide excellent qualitative matches to the experimental data. This work considerably extends the scope of XUV spectroscopy and establishes it as a potentially transformative tool for mainstream research in inorganic, bioinorganic, and organometallic chemistry.

Extreme ultraviolet photons are produced through the process of high-harmonic generation.[20,21] As shown in Figure 1, a Ti:sapphire laser (800 nm, 4 mJ, 35 fs, 1 kHz) is focused into a semi-infinite gas cell[22] containing Ne gas, where the intense electromagnetic field at the focal point ionizes the Ne, accelerates the free electrons, then drives them back into the ionized atoms. This process produces ∼20 fs pulses of XUV

Received: June 23, 2016
Accepted: August 11, 2016

DOI: 10.1021/acs.jpclett.6b01393
J. Phys. Chem. Lett. 2016, 7, 3383−3387

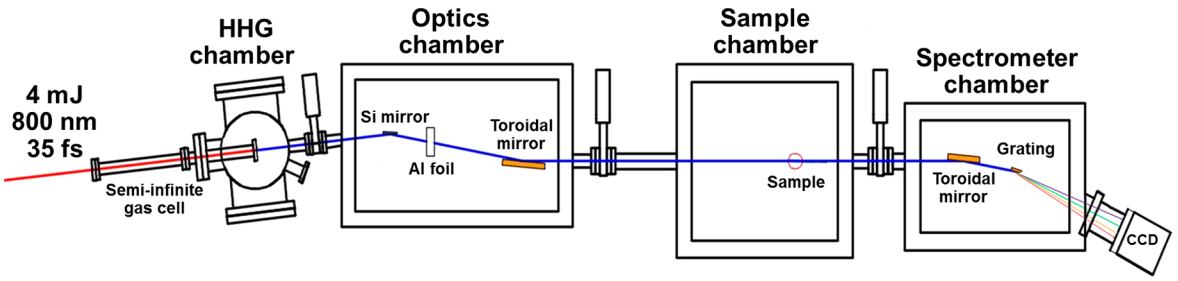

Figure 1. Diagram of the XUV absorption instrument. XUV photons are created via high-harmonic generation, focused to the sample using a toroidal mirror, then dispersed onto an array CCD. A Si mirror and 200 nm thick Al foil absorb the residual 800 nm light.

photons in the 45−100 eV energy range. A Si mirror followed by an Al foil block the residual 800 nm light and XUV photons above 72 eV. At the sample, the flux is ~10^6 photons/s/0.1 eV, approximately a factor of 10^8 lower than that of undulator beamlines at storage rings. After passing through the sample, the light is dispersed by a grating onto an array CCD, allowing a full spectrum to be collected at once. The entire system fits onto a 10-by-22 foot L-shaped laser table.

As shown in Figure 2A, high-harmonic generation produces a broad XUV continuum with peaks at odd harmonics of the 800

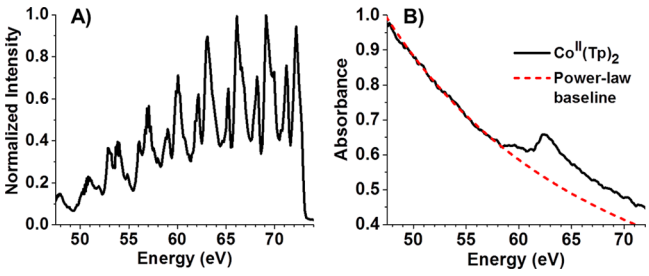

Figure 2. (A) XUV continuum produced by high-harmonic generation. (B) Raw absorption spectrum of $Co^{II}(Tp)_2$. The Co $M_{2,3}$ edge near 60 eV appears on top of a power-law baseline caused by valence electron photoionization. Photons with energy above 72 eV are blocked by the Al foil used to attenuate the 800 nm driving pulse.

nm driving field (every 3.1 eV). A raw absorption spectrum (sample minus blank, see Supporting Information) consists of resonant features at the metal $M_{2,3}$ edge on top of a broad nonresonant sloping background caused by photoionization of metal and ligand valence electrons (Figure 2B). The spectra shown are the average of three to four spectra collected on different days, each collected in 1 to 5 min (day-to-day fluctuations are shown in Figure S7). The low-energy region below the absorption edge is fit to a power law, and this baseline is subtracted. Finally, for ease of comparison between species, each spectrum is normalized to 1 at the highest point. More rigorous normalization, as performed for L-edge spectra using both the pre-edge and post-edge intensity,[23] is difficult due to the Fano line shape (see below) and the experimental cutoff at 72 eV. Sum rules dictate that the total integrated absorption is proportional to the number of unoccupied d orbitals, so a more detailed treatment of normalization could help to confirm the oxidation state assignments described below.

Five model complexes (Chart 1) have been chosen to demonstrate the sensitivity of M-edge XANES to the metal identity, oxidation state, spin state, and ligand field. Samples are deposited as ~100 nm thick films on 100 nm Si_3N_4 substrates. Experimental and simulated spectra of the model complexes are

Chart 1. Model Complexes

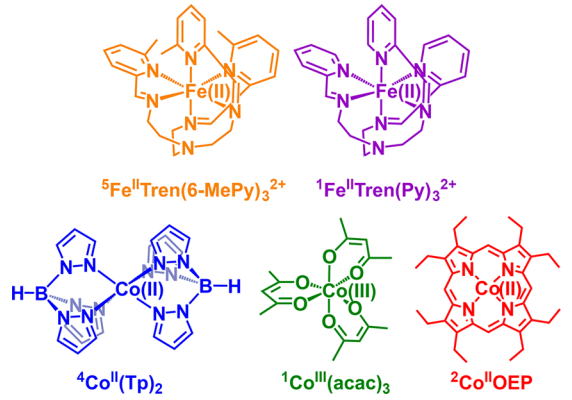

shown in Figure 3. Simulated spectra are computed using the ligand-field multiplet (LFM) model that takes into account angular momentum coupling between 3d electrons and the 2p/3p core hole. This model has been widely used to treat $L_{2,3}$ edge spectra,[3] and has been applied to a handful of $M_{2,3}$-edge spectra of inorganic complexes.[24−27] The crystal field splitting parameter 10Dq for each complex was taken from UV/visible data or $L_{2,3}$-edge studies. Calculated spectra are broadened with a Gaussian function to account for the spectrometer resolution (σ = 0.2 eV), with a Fano line shape to account for interference between direct 3d photoionization and 3p3d3d Auger emission (q = 3.5)[26] and with a Lorentzian function to account for the intrinsic lifetime of each final state. These lifetimes are calculated directly, assuming that the predominant decay pathway is Auger emission. Absolute transition energies calculated by the LFM method carry systematic errors of 1−5 eV. The Fe spectra have been shifted by +3.3 eV to match the highest peak in ^{5}**Fe^{II}Tren(6-MePy)**$^{2+}$, but the two simulations have not been shifted relative to each other. The Co simulations have not been shifted from the calculated energy scale. In future work we will calibrate these shifts using additional model complexes. Further details are provided in the Supporting Information.

The spectra of the octahedral complexes ^{5}**Fe^{II}Tren(6-MePy)**$^{2+}$ and ^{1}**Fe^{II}Tren(Py)**$_3^{2+}$ in Figure 3A show the sensitivity of M-edge XANES to spin state. ^{1}**Fe^{II}Tren(Py)**$_3^{2+}$ is low-spin, whereas ^{5}**Fe^{II}Tren(6-MePy)**$_3^{2+}$ is high-spin; in the latter, the methyl groups on the pyridyl rings distort the coordination geometry and weaken the ligand field. These two complexes straddle the high-spin/low-spin crossover point for octahedral d^6 complexes and have previously been used as models in studies of photoinduced spin switching.[28] The experimental spectrum of ^{5}**Fe^{II}Tren(6-MePy)**$_3^{2+}$ contains a peak at 57.6 eV, with a possible low energy shoulder at 55.6 eV.

DOI: 10.1021/acs.jpclett.6b01393
J. Phys. Chem. Lett. 2016, 7, 3383−3387

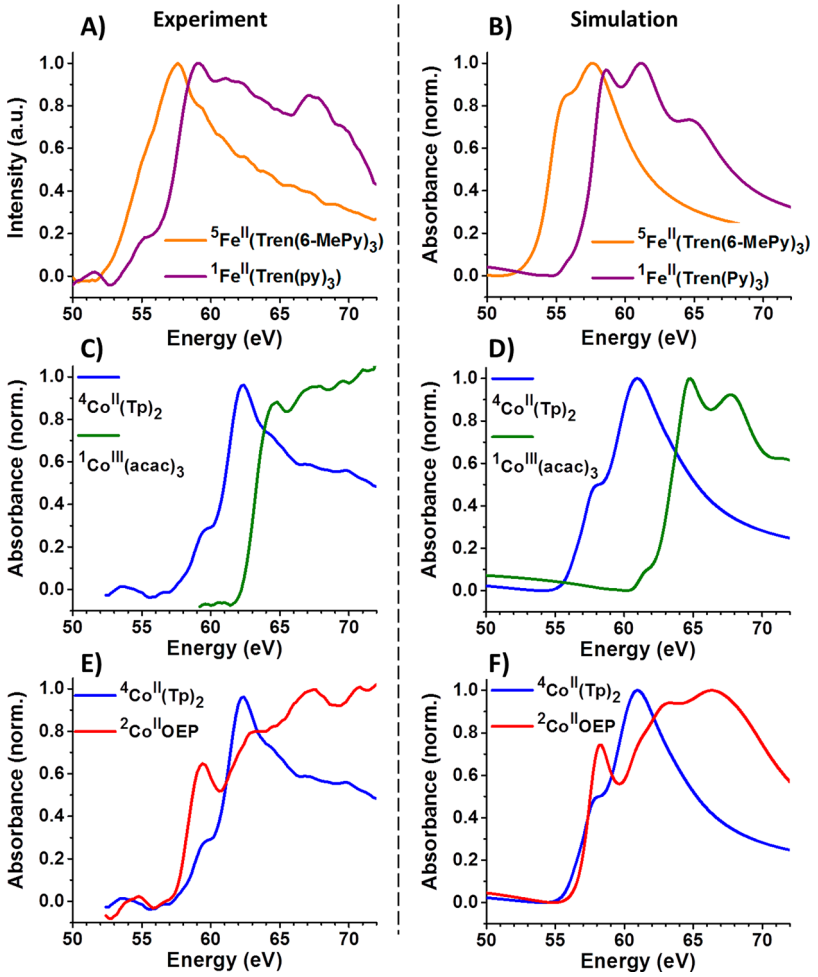

Figure 3. Normalized absorption spectra of model compounds. (A) Experimental and (B) simulated spectra of high-spin $^5Fe^{II}Tren(6\text{-}MePy)_3^{2+}$ and low-spin $^1Fe^{II}Tren(Py)_3^{2+}$, showing spin state specificity. (C) Experimental and (D) simulated spectra of octahedral $^4Co^{II}(Tp)_2$ and $^1Co^{III}(acac)_3$, showing oxidation state specificity. (E) Experimental and (F) simulated spectra of octahedral $^4Co^{II}(Tp)_2$ and square planar $^2Co^{II}OEP$, showing ligand field specificity.

The spectrum of low-spin $^1\mathbf{Fe^{II}Tren(Py)_3}^{2+}$ is blue-shifted by ~2.5 eV (as judged by the energy of the rising edge at half height), with a small shoulder at 55.2 eV and peaks at 59.0, 61.6, and 67.4 eV. A similar blue shift is seen at the $L_{2,3}$-edge between high- and low-spin octahedral Fe^{II} complexes and is attributed to greater exchange stabilization of the core hole in the high-spin case.[8,25]

The simulated spectrum of high-spin $^5\mathbf{Fe^{II}Tren(6\text{-}MePy)_3}^{2+}$ in Figure 3B contains a shoulder at 55.6 eV and a peak at 57.6. This reasonably matches the shoulder-to-peak spacing seen experimentally, although the shoulder is significantly stronger and better resolved in the simulation. The simulated spectrum of low-spin $^1\mathbf{Fe^{II}Tren(Py)_3}^{2+}$ shows a weak shoulder at 55.9 eV and peaks at 58.6, 61.2, and 64.6 eV. For this complex, the general shape of the calculated spectrum matches that seen experimentally, although the peak-to-peak spacing is compressed in the simulation relative to the experiment. Note that the $3p_{1/2}$ and $3p_{3/2}$ core-hole levels are separated by <1 eV, so separate M_2 and M_3 edges are not observed (unlike the L_2 and L_3 edges). Detailed assignments of the absorption peaks are given in the Supporting Information.

The spectra of the octahedral complexes $^4\mathbf{Co^{II}(Tp)_2}$ and $^1\mathbf{Co^{III}(acac)_3}$ in Figure 3C show the sensitivity of M-edge XANES to oxidation state. The spectrum of $^4\mathbf{Co^{II}(Tp)_2}$ has a peak at 62.4 eV with a well-defined low-energy shoulder at 59.8 eV. The spectrum of $^1\mathbf{Co^{III}(acac)_3}$ is blue-shifted by ~3 eV, with peaks at 64.7 and 67.4 eV; a possible third peak is seen at 71 eV. The 3p binding energy in Co^{III} complexes is ~1 eV greater than that of Co^{II},[29,30] so the 3 eV blue-shift shift is likely due to the additive effect of the oxidation state and spin state changes. The edge shift due to spin state changes is similar in magnitude to the shift from oxidation state changes, so both peak position and shape must be used for electronic state assignment. Within a given oxidation and spin state, changes in molecular structure may also shift the edge. However, the rough spectral shape and position is fairly robust, as shown in Figure S1 for additional model complexes $(Bu_4N)_2(Co^{II}Cl_4)$ and $[Co^{III}(Tp)_2]Br$. Future work will explore the sensitivity of M-edge XANES to small changes in symmetry, ligand field strength, and covalency. Note that the spectrum of d^6 low-spin $^1\mathbf{Fe^{II}Tren(Py)_3}^{2+}$ is red-shifted by 5 eV from that of the isoelectronic $^1\mathbf{Co^{III}(acac)_3}$, showing the element specificity at this edge.

The shapes of the $^4\mathbf{Co^{II}(Tp)_2}$ and $^1\mathbf{Co^{III}(acac)_3}$ spectra are reproduced well in the ligand field multiplet simulations shown in Figure 3D, although the blue shift upon oxidation is exaggerated. The $^4\mathbf{Co^{II}(Tp)_2}$ simulation consists of a main peak at 60.9 eV with a low-energy shoulder at 58.1 eV; the shoulder-

DOI: 10.1021/acs.jpclett.6b01393
J. Phys. Chem. Lett. 2016, 7, 3383−3387

peak separation of 2.8 eV is an excellent match for the experimental value of 2.7 eV The simulation of $^{1}Co^{III}(acac)_3$ shows a sharp rise, followed by three peaks at 64.8, 67.7, and 71.3 eV. As with $^{4}Co^{II}(Tp)_2$, these are close matches to the experimental data. All of the simulations in this work underestimate the absorption intensity at high energy due to neglect of 3p photoionization, as discussed in Section 4 of the Supporting Information.

Figure 3E,F shows the ligand field sensitivity of M-edge XANES by comparing the spectrum of octahedral $^{4}Co^{II}(Tp)_2$ with that of square-planar $^{2}Co^{II}OEP$. Although the rising edges of both complexes begin at 57.6 eV, the latter shows a strong, well-defined peak at 59.4 eV, followed by peaks at 63.2 and 67.4 eV. The differences seen experimentally in the spectra of the two complexes are again reproduced in the simulations (Figure 3D). Note that the change in ligand field symmetry is accompanied by a change in the spin state of the complex.

The sensitivity of M-edge spectroscopy to the electronic structure of first-row transition-metal complexes was predicted as early as 1991[25] and observed in transition-metal oxides[14−16,31] and halides[26,27] but until now has not been demonstrated in molecular systems. There are two fundamental challenges to absorption spectroscopy at the M edge, as compared to the L and K edges. First, the penetration depth of XUV photons is an order of magnitude lower than that of soft X-rays due to photoionization of valence electrons (this is the downside to the high oscillator strength discussed earlier as a benefit for pump−probe spectroscopy). Although the low penetration depth of XUV photons was not a major roadblock for studying inorganic solids with a high metal-to-nonmetal ratio,[14−16,31] the complexes studied here contain one metal atom per ∼30 ligand atoms, all of which attenuate the XUV beam. Second, 3p core holes have Auger lifetimes of <1 fs due to the large 3p3d3d overlap integral (super Coster−Kronig transition).[32] M-edge absorption peaks therefore have intrinsic line widths of 1 to 2 eV, which are twice as broad as $L_{2,3}$-edge absorption peaks. Overlap between broad peaks might be expected to smear out any identifying features in the spectra.

This work shows that these disadvantages can be overcome and that the weak resonant signal from the metal can be successfully isolated from the strong nonresonant background (Figure 2B). Multiple peaks or shoulders are observed in the spectra, showing that the inherently large line widths at this edge do not impede identification of the electronic structure of molecular complexes. The position of the absorption edge is sensitive to the oxidation state and spin state of the complex as well as the identity of the ligands, with shifts consistent with those seen at L and K edges. Ligand field multiplet simulations provide excellent qualitative matches with the experimental results, and in all cases but $^{1}Fe^{II}Tren(Py)_3^{2+}$ the peak-to-peak spacings are within a few tenths of an electronvolt of the experimental values. Addition of charge-transfer effects, fine-tuning of the ligand field parameters, and calibration of the calculated edge positions may improve the accuracy of the simulations, although the Fano line shape will pose a challenge in the post-edge region. Ab initio calculations have shown excellent results for both K-edge[33,34] and L-edge spectra,[35,36] and the latter codes should be transferable to the M edge.

This work opens the possibility of M-edge XANES as a routine characterization technique for the inorganic, bio-inorganic, and organometallic communities. The oxidation state, spin state, and ligand field symmetry of transition-metal complexes can be measured in minutes using instrumentation accessible to most ultrafast spectroscopy laboratories. Finally, the inherent femtosecond time resolution of this technique will enable transition-metal photophysics to be measured on ultrafast time scales. Such studies have already been performed on transition-metal oxides[14−16] and may now be extended to molecular complexes relevant to light harvesting and catalysis.

■ ASSOCIATED CONTENT

Supporting Information

The Supporting Information is available free of charge on the ACS Publications website at DOI: 10.1021/acs.jpclett.6b01393.

Sample preparation, further examples of oxidation state specificity, details of ligand field multiplet calculations, peak shapes, and peak assignments, description of data collection procedures, raw spectra before baseline subtraction, and subtracted spectra with noise. (PDF)

■ AUTHOR INFORMATION

Corresponding Author

*E-mail: vuraweis@illinois.edu.

Notes

The authors declare no competing financial interest.

■ ACKNOWLEDGMENTS

This material is based on work supported by the Air Force Office of Scientific Research under AFOSR Award No. FA9550-14-1-0314 to J.V.-W. and NSF CHE 13-62931 to G.S.G. We would like to dedicate this paper in memory of Robert Brown, whose skillful machining made this work possible.

■ REFERENCES

(1) Solomon, E. I.; Szilagyi, R. K.; DeBeer George, S.; Basumallick, L. Electronic Structures of Metal Sites in Proteins and Models: Contributions to Function in Blue Copper Proteins. *Chem. Rev.* **2004**, *104*, 419−458.

(2) Garino, C.; Borfecchia, E.; Gobetto, R.; van Bokhoven, J. A.; Lamberti, C. Determination of the Electronic and Structural Configuration of Coordination Compounds by Synchrotron-Radiation Techniques. *Coord. Chem. Rev.* **2014**, *277−278*, 130−186.

(3) de Groot, F. M. F.; Kotani, A. *Core Level Spectroscopy of Solids*; CRC Press, 2008.

(4) Bordiga, S.; Groppo, E.; Agostini, G.; van Bokhoven, J. A.; Lamberti, C. Reactivity of Surface Species in Heterogeneous Catalysts Probed by In Situ X-Ray Absorption Techniques. *Chem. Rev.* **2013**, *113* (3), 1736−1850.

(5) Chen, L. X. Probing Transient Molecular Structures in Photochemical Processes Using Laser-Initiated Time-Resolved X-Ray Absorption Spectroscopy. *Annu. Rev. Phys. Chem.* **2005**, *56*, 221−254.

(6) Bressler, C.; Chergui, M. Ultrafast X-Ray Absorption Spectroscopy. *Chem. Rev.* **2004**, *104* (4), 1781−1812.

(7) Milne, C. J.; Penfold, T. J.; Chergui, M. Recent Experimental and Theoretical Developments in Time-Resolved X-Ray Spectroscopies. *Coord. Chem. Rev.* **2014**, *277−278*, 44−68.

(8) Huse, N.; Cho, H.; Hong, K.; Jamula, L.; de Groot, F. M. F.; Kim, T. K.; McCusker, J. K.; Schoenlein, R. W. Femtosecond Soft X-Ray Spectroscopy of Solvated Transition-Metal Complexes: Deciphering the Interplay of Electronic and Structural Dynamics. *J. Phys. Chem. Lett.* **2011**, *2*, 880−884.

(9) Smolentsev, G.; Sundström, V. Time-Resolved X-Ray Absorption Spectroscopy for the Study of Molecular Systems Relevant for Artificial Photosynthesis. *Coord. Chem. Rev.* **2015**, *304*, 117−132.

(10) Turgut, E.; La-o-Vorakiat, C.; Shaw, J. M.; Grychtol, P.; Nembach, H. T.; Rudolf, D.; Adam, R.; Aeschlimann, M.; Schneider, C. M.; Silva, T. J.; et al. Controlling the Competition between

DOI: 10.1021/acs.jpclett.6b01393
J. Phys. Chem. Lett. 2016, 7, 3383−3387

Optically Induced Ultrafast Spin-Flip Scattering and Spin Transport in Magnetic Multilayers. *Phys. Rev. Lett.* **2013**, *110*, 197201.
(11) La-O-Vorakiat, C.; Siemens, M.; Murnane, M. M.; Kapteyn, H. C.; Mathias, S.; Aeschlimann, M.; Grychtol, P.; Adam, R.; Schneider, C. M.; Shaw, J. M.; et al. Ultrafast Demagnetization Dynamics at the M Edges of Magnetic Elements Observed Using a Tabletop High-Harmonic Soft X-Ray Source. *Phys. Rev. Lett.* **2009**, *103*, 257402.
(12) Loh, Z.-H.; Leone, S. R. Ultrafast Strong-Field Dissociative Ionization Dynamics of CH_2Br_2 Probed by Femtosecond Soft X-Ray Transient Absorption Spectroscopy. *J. Chem. Phys.* **2008**, *128*, 204302.
(13) Goulielmakis, E.; Loh, Z. H.; Wirth, A.; Santra, R.; Rohringer, N.; Yakovlev, V. S.; Zherebtsov, S.; Pfeifer, T.; Azzeer, A. M.; Kling, M. F.; et al. Real-Time Observation of Valence Electron Motion. *Nature* **2010**, *466*, 739−743.
(14) Vura-Weis, J.; Jiang, C.-M.; Liu, C.; Gao, H.; Lucas, J. M.; de Groot, F. M. F.; Yang, P.; Alivisatos, A. P.; Leone, S. R. Femtosecond $M_{2,3}$-Edge Spectroscopy of Transition-Metal Oxides: Photoinduced Oxidation State Change in α-Fe_2O_3. *J. Phys. Chem. Lett.* **2013**, *4*, 3667−3671.
(15) Jiang, C.-M.; Baker, L. R.; Lucas, J. M.; Vura-Weis, J.; Alivisatos, A. P.; Leone, S. R. Characterization of Photo-Induced Charge Transfer and Hot Carrier Relaxation Pathways in Spinel Cobalt Oxide (Co_3O_4). *J. Phys. Chem. C* **2014**, *118*, 22774−22784.
(16) Baker, L. R.; Jiang, C.-M.; Kelly, S. T.; Lucas, J. M.; Vura-Weis, J.; Gilles, M. K.; Alivisatos, A. P.; Leone, S. R. Charge Carrier Dynamics of Photoexcited Co_3O_4 in Methanol: Extending High Harmonic Transient Absorption Spectroscopy to Liquid Environments. *Nano Lett.* **2014**, *14*, 5883−5890.
(17) Popmintchev, T.; Chen, M. C.; Popmintchev, D.; Arpin, P.; Brown, S.; Alisauskas, S.; Andriukaitis, G.; Balciunas, T.; Mucke, O. D.; Pugzlys, A.; et al. Bright Coherent Ultrahigh Harmonics in the keV X-Ray Regime from Mid-Infrared Femtosecond Lasers. *Science (Washington, DC, U. S.)* **2012**, *336*, 1287−1291.
(18) Weisshaupt, J.; Juvé, V.; Holtz, M.; Ku, S.; Woerner, M.; Elsaesser, T.; Ališauskas, S.; Pugžlys, A.; Baltuška, A. High-Brightness Table-Top Hard X-Ray Source Driven by Sub-100-Femtosecond Mid-Infrared Pulses. *Nat. Photonics* **2014**, *8*, 927−930.
(19) Gerasimova, N.; Dziarzhytski, S.; Feldhaus, J. The Monochromator Beamline at FLASH: Performance, Capabilities and Upgrade Plans. *J. Mod. Opt.* **2011**, *58*, 1480−1485.
(20) Corkum, P. B. Plasma Perspective on Strong-Field Multiphoton Ionization. *Phys. Rev. Lett.* **1993**, *71*, 1994−1997.
(21) Loh, Z. H.; Leone, S. R. Capturing Ultrafast Quantum Dynamics with Femtosecond and Attosecond X-Ray Core-Level Absorption Spectroscopy. *J. Phys. Chem. Lett.* **2013**, *4*, 292−302.
(22) Sutherland, J. R.; Christensen, E. L.; Powers, N. D.; Rhynard, S. E.; Painter, J. C.; Peatross, J. High Harmonic Generation in a Semi-Infinite Gas Cell. *Opt. Express* **2004**, *12*, 4430−4436.
(23) Wasinger, E. C.; de Groot, F. M. F.; Hedman, B.; Hodgson, K. O.; Solomon, E. I. L-Edge X-Ray Absorption Spectroscopy of Non-Heme Iron Sites: Experimental Determination of Differential Orbital Covalency. *J. Am. Chem. Soc.* **2003**, *125*, 12894−12906.
(24) Berlasso, R.; Dallera, C.; Borgatti, F.; Vozzi, C.; Sansone, G.; Stagira, S.; Nisoli, M.; Ghiringhelli, G.; Villoresi, P.; Poletto, L.; et al. High-Order Laser Harmonics and Synchrotron Study of Transition Metals $M_{2,3}$ Edges. *Phys. Rev. B: Condens. Matter Mater. Phys.* **2006**, *73*, 115101.
(25) van der Laan, G. $M_{2,3}$ Absorption-Spectroscopy of 3d Transition-Metal Compounds. *J. Phys.: Condens. Matter* **1991**, *3*, 7443−7454.
(26) Shin, S.; Suga, S.; Kanzaki, H.; Shibuya, S.; Yanaguchi, T. Multiplet Structures of the Inner Core Absorption-Spectra of $KMnF_3$ and $KCoF_3$ Measured by Synchrotron Radiation. *Solid State Commun.* **1981**, *38*, 1281−1284.
(27) Wang, H.; Young, A. T.; Guo, J.; Cramer, S. P.; Friedrich, S.; Braun, A.; Gu, W. Soft X-Ray Absorption Spectroscopy and Resonant Inelastic X-Ray Scattering Spectroscopy below 100 eV: Probing First-Row Transition-Metal M-Edges in Chemical Complexes. *J. Synchrotron Radiat.* **2013**, *20*, 614−619.
(28) Huse, N.; Cho, H.; Hong, K.; Jamula, L.; de Groot, F. M. F.; Kim, T. K.; McCusker, J. K.; Schoenlein, R. W. Femtosecond Soft X-Ray Spectroscopy of Solvated Transition-Metal Complexes: Deciphering the Interplay of Electronic and Structural Dynamics. *J. Phys. Chem. Lett.* **2011**, *2*, 880−884.
(29) Strydom, C. A.; Strydom, H. J. X-Ray Photoelectron Spectroscopy Studies of Some cobalt(II) Nitrate Complexes. *Inorg. Chim. Acta* **1989**, *159*, 191−195.
(30) Burger, K.; Ebel, H.; Ebel, M.; Várhelyi, C. XPS Study of Low-Spin cobalt(III) Mixed Ligand Complexes. *Inorg. Chim. Acta* **1984**, *88*, L11−L13.
(31) van Aken, P. A.; Styrsa, V. J.; Liebscher, B.; Woodland, A. B.; Redhammer, G. J. Microanalysis of Fe3+/ΣFe in Oxide and Silicate Minerals by Investigation of Electron Energy-Loss near-Edge Structures (ELNES) at the Fe $M_{2,3}$ Edge. *Phys. Chem. Miner.* **1999**, *26*, 584−590.
(32) Davis, L. C.; Feldkamp, L. A. Interpretation of 3p-Core-Excitation Spectra in Cr, Mn, Fe, Co, and Ni. *Solid State Commun.* **1976**, *19*, 413−416.
(33) Rehr, J. J.; Ankudinov, A. L. Progress in the Theory and Interpretation of XANES. *Coord. Chem. Rev.* **2005**, *249*, 131−140.
(34) Guda, S. A.; Guda, A. A.; Soldatov, M. A.; Lomachenko, K. A.; Bugaev, A. L.; Lamberti, C.; Gawelda, W.; Bressler, C.; Smolentsev, G.; Soldatov, A. V.; et al. Optimized Finite Difference Method for the Full-Potential XANES Simulations: Application to Molecular Adsorption Geometries in MOFs and Metal−Ligand Intersystem Crossing Transients. *J. Chem. Theory Comput.* **2015**, *11*, 4512−4521.
(35) Josefsson, I.; Kunnus, K.; Schreck, S.; Fohlisch, A.; de Groot, F.; Wernet, P.; Odelius, M. Ab Initio Calculations of X-Ray Spectra: Atomic Multiplet and Molecular Orbital Effects in a Multiconfigurational SCF Approach to the L-Edge Spectra of Transition Metal Complexes. *J. Phys. Chem. Lett.* **2012**, *3*, 3565−3570.
(36) Maganas, D.; DeBeer, S.; Neese, F. Restricted Open-Shell Configuration Interaction Cluster Calculations of the L-Edge X-Ray Absorption Study of TiO2 and CaF2 Solids. *Inorg. Chem.* **2014**, *53*, 6374−6385.

DOI: 10.1021/acs.jpclett.6b01393
J. Phys. Chem. Lett. 2016, 7, 3383−3387